Indian Journal of Chemistry
Vol. 60A, February 2021, pp. 209-219

Application of the graphene oxide/chitosan nanocomposite in the removal of methyl orange from aqueous solutions: a mechanism study

Mina Azadfar[a], Hasan Tahermansouri[b,]* & Mahnaz Qomi[c]

[a]Department of Organic Chemistry, Faculty of Pharmaceutical Chemistry, Tehran Medical Sciences, Islamic Azad University, Tehran, Iran

[b]Department of Chemistry, Ayatollah Amoli Branch, Islamic Azad University, Amol, Iran

[c]Active Pharmaceutical Ingredients Research Center (APIRC), Tehran Medical Sciences, Islamic Azad University, Tehran, Iran

*E-mail: h.tahermansuri@iauamol.ac.ir/ tahermansuri@yahoo.com

Received 14 February 2020; revised and accepted 07 December 2020

Graphene oxide (GO) and the functionalized graphene oxide with chitosan (GO-C) has been used for the removal of methyl orange from aqueous solutions. Batch experiments such as solution pH, amount of adsorbents, contact time, concentration of the methyl orange and temperature are carried out to study the sorption process. Kinetic studies are well described by pseudo-second-order kinetic model for both adsorbents. Isotherm studies have shown that Langmuir isotherm for GO and GO-C are the best to represent the measured sorption data. Negative ΔG° values indicate the nature of spontaneous adsorption process. Physical sorption is suggested for the adsorption process. In addition, methyl orange molecules can be desorbed from GO-C up to 79.2% at pH =11 and that the consumed GO-C can be reutilized up to 5th cycle of regeneration.

Keywords: Adsorption isotherms, Desorption, Graphene oxide, Chitosan, Methyl orange, Thermodynamic

One of the distinguished acidic/anionic dyes is methyl orange which has been extensively utilized in textile, printing, paper, plastics, rubber, cosmetics, food and pharmaceutical industries and research laboratories[1,2]. However, it culminates in health hazards such as vomiting, diarrhea, breathing and nausea since as a weak acid base indicator it is toxic and carcinogenic agent[3]. Moreover, low biodegradability of methyl orange is an important topic for environmental science[4]. Therefore, the removal and elimination of methyl orange from various aqueous solutions are essential. So far, the various methods were presented for the removal of dyes from contaminated water which can be cited adsorption[5], electrochemical method[6], ion exchange[7], degradation[8], photocatalytic degradation[9], coagulation-flocculation[10], biological treatment[11] and membrane separation[12]. Among these approaches, adsorption process has been known as an effective technique with high efficiency and capacity to remove dyes[13]. Besides, this method has the potential for regeneration, recovery, and recycling of adsorbents in comparison to other methods.

In recent years, a great number of studies have been reported for the removal of methyl orange from aqueous solutions by different adsorbents such as molybdenum disulfide[14], nanocomposites[15,16], nanoparticles[17,18], biochar[19], carbon nanomaterials[20], graphene oxide[21], pumpkin seed[22] and actived carbon[23]. Furthermore, metal organic frameworks (MOFs), mesoporous silica and periodic mesoporous organosilicas (PMOs) with different functionalities have been extensively considered as significant adsorbents[24-29]. For example, cyclophosphazene bridged mesoporous organosilicas (CPMOs) were applied for the adsorption of organic dyes such as methyl orange (523 mg g^{-1}), congo red (320 mg g^{-1}) and Cr(VI) ions (101 mg g^{-1}).[24] In other research, organosilica with a low surface area was used for the adsorptive removal of $Cr_2O_7^{2-}$ and methyl orange with adsorption capacity of 359 and 1679 mg g^{-1}, respectively.[25] Nanoporous hypercrosslinked polyaniline (HCPANI) was studied as an efficient adsorbent to remove both crystal violet and methyl orange dyes where its adsorption capacity was reported about 245 and 220 mg g^{-1} for crystal violet and methyl orange, respectively[26]. In other study, nitrogen enriched triazine bridged mesoporous organosilicas (NETPMOs) adsorbed methyl orange

with adsorption capacity about 1262 mg g^{-1} at pH= 7[27]. Table 1 shows adsorption capacity of some adsorbents for the removal of methyl orange under different experimental conditions.

Among these adsorbents, carbon nanomaterials such as graphene and carbon nanotubes are famous for this issue and have been utilized as good adsorbents[40-42]. Graphene oxide (GO) is an oxygen-rich carbonaceous layered material which is a kind of important derivatives of graphene. A large numbers of oxygenated functionalities and high surface area of GO are the most important character for the adsorption process. Nonetheless, adsorption performance of GO with chitosan can be further improved[43]. In fact, graphene oxide-chitosan (GO-C) composites have been developed to removal pollutions from wastewater. Hence, the remarkable review articles have been devoted to this topic[44-46].

Taking this background into account and considering the toxic activities of methyl orange for humans, the purpose of the present work was to study the removal of methyl orange from aqueous solutions by GO-C nanocomposite. In this current study, GO-C nanocomposite was applied as an efficient adsorbent for the removal of the methyl orange from aqueous solutions. In this research, the different kinetic models such as, pseudo-first order, pseudo-second-order, intra-particle diffusion and Elovich and six adsorption isotherm models (Langmuir, Freundlich, Halsey, Tempkin,Harkins-Jura, Dubinin-Radushkevich) were studied to get an adequate understanding on the mechanism and rate of the adsorption process of methyl orange on the GO-C. In fact, the goal of this investigation was to compare GO and GO-C nanocomposite as adsorbent for removal of methyl orange from aqueous solutions.

Materials and Methods

Chitosan with low molecular weight (MW = 1.08×10^5, degree of deacetylation = 81%) from Sigma-Aldrich, methyl orange, ammonia and glutaraldehyde (GLA) from Merck Chemical Inc. and graphene oxide nanoplatelets (99%, thickness 3.4–7 nm with 6-10 Layers) were purchased and used as received. Analytical reagent-grade chemicals were used as well as deionized water from a Milli-Q system (Millipore). The concentration of methyl orange was determined by Unico UV-2100 Model variable-wavelength UV-visible spectrophotometer at 470 nm. Field emission scanning electron microscopic images were taken using a MIRA3\\TESCAN-XMU model.

Synthesis of GO-C nanocomposite

We reported the GO-C synthesis in our previous paper [41]. However, 0.5 g of GO with 200 mL of chitosan solution (0.5 g of chitosan dissolved in 500 mL of 2% (v/v) acetic acid solution) was mixed and stirred for 2 h. Then, the pH of the reaction mixture was adjusted to 10-11 and was heated to 60 °C for further 1 h. Afterward, 1 mL of GLA was added into the reaction mixture for the cross-linking of chitosan and the mixed system was stirred continuously for other 1h. Black products was collected by centrifugation and washed with diluted acetic acid and distilled water to remove uncross-

Table 1 — Literature results of the methyl orange adsorption by different adsorbents

Adsorbents	Adsorption capacity (mg/g)	Refs.
Graphene oxide	16.83	21
CPMOs	523	24
organosilica	1679	25
HCPANI	220	26
NETPMOs	1262	27
Zeolite NaA/CuO	79.49	30
KGM/GO	51.6	31
pomelo peel	680.2	32
Poly 2- hydroxyethyl methacrylate –chitosan-MWCNT nanocomposite	306.1	33
Calcium alginate MWCNTs	12.5	34
Blast furnace slag acid-alkali precipitate (BFSMP)	167	35
Zirconium-immobilized bentonite	44.13	36
goethite impregnated with chitosan beads (GCSB)	84	37
Chitosan intercalated montmorillonite	95.55	38
Chitosan- graphene oxide aerogels	686.89	39
GO-C	107	This work

linked chitosan. Finally, the black powder of the obtained GO-C was dried at 60 °C overnight.

Batch sorption experiments

To study the effects of pH on the sorption of methyl orange, 30 mg of GO or GO-C was dispersed into 30 mL solutions containing 100 mg/L of methyl orange. The initial pH values were adjusted from 3.0 to 9.0 using nitric acid and NaOH at 25±1 °C. The amounts of sorbed methyl orange were calculated as the difference between the initial and final concentrations when the equilibrium was reached. The results are based on at least three replicate experiments for each pH value. To estimate the sorption capacity, 30 mg of GO or GO-C was mixed with 50 mL of methyl orange solution (concentration range 10-100 mg/L). After 90 min, the methyl orange concentration was determined by UV-visible absorption spectroscopy. The adsorption (%) and sorption capacity q (mg/g) was obtained as follows in Eqns (1) and (2):

$$Adsorption\ \% = \frac{C_0 - C_e}{C_0} \times 100 \quad \ldots (1)$$

$$q_e = \frac{(C_0 - C_e) \times V}{m} \quad \ldots (2)$$

where, C_0 and C_e are the initial and final concentrations (mg/L) of methyl orange in the solution, respectively, V (L) is the volume of methyl orange solution and m (g) is the weight of sorbent. The kinetic experiments were carried out under normal atmospheric conditions at 25±1 °C. Initially, 30 mg of GO or GO-C was contacted with 50 mL solution containing 100 mg L^{-1} methyl orange concentration in glass vials and then it was stirred for the different times. Adsorbent and solution were separated at predetermined time intervals, filtered using a 0.45 µm membrane filter and analyzed for residual methyl orange concentrations as described above. The thermodynamic experiments were carried out at different temperatures (25, 40 and 50 °C) and the used values were similar to kinetic ones.

Desorption and reuse of GO-C

The adsorption was done in 50 mL of 100 mg L^{-1} methyl orange solution at pH of 3 with 30 mg of GO-C at 298 K for 90 min. After filtration, the GO-C was immersed in 50 mL of 1 mol L^{-1}NaOH or HNO_3 and agitated at 298 K for 90 min. Then, the GO-C was removed from the solution and washed with water. Thus, released methyl orange values in the solution were determined by above equations.

Non-linear regression analysis

The adsorption equilibrium data for methyl orange onto GO and GO-C were analyzed by non-linear curve fitting analysis, using MATLAB® software, to fit the kinetic and isotherm models. The optimization procedure requires an error function to be defined in order to be able to evaluate the fit of the equation to the experimental data. Coefficient of determination (R^2) and residual root mean square error (RMSE) were used to measure the goodness-of-fit[28]. The R^2 (Eqn (3)) and RMSE (Eqn (4)) can be defined as:

$$R^2 = \frac{\sum (q_{e,cal} - \bar{q}_{e,ex})^2}{\sum (q_{e,cal} - \bar{q}_{e,ex})^2 + \sum (q_{e,cal} - q_{e,ex})^2} \quad \ldots (3)$$

$$RMSE = \sqrt{\frac{1}{n-2} \sum_{i=1}^{i=n} (q_{e,ex} - q_{e,cal})^2} \quad \ldots (4)$$

where, $q_{e,ex}$, $q_{e,cal}$ and $\bar{q}_{e,ex}$ are the experimental, calculated and the average of $q_{e,ex}$ values, respectively, and n is the number of measurements. Higher R^2 and smaller RMSE values indicates the better curve fitting.

Results and Discussion

Characterization of adsorbents

The different techniques are applied for the characterization of GO-C such as FT-IR, TGA, DTG and BET which we explained in our previous report [41]. Fig. 1 shows SEM images of GO and GO-C. According to Fig. 1, SEM image of GO seems like the sheet-like arrangement, smooth surface, and wrinkled edge while that of GO-C presents insertion of chitosan between the graphene layers which demonstrate the modification of the GO layers with chitosan.

Adsorption studies

pH effect

PH effect on the adsorption of methyl orange by GO and GO-C in the range 3.0 to 9 is shown in Fig. 2. According to Fig. 2, diminishing pH values culminate in raising the adsorption of methyl orange by both adsorbents such that the maximum of adsorption is discernible at pH=3. For example, at pH 3 and 9 methyl orange removed by GO was about 44.9% and 12.7%, respectively, while amounts of methyl orange

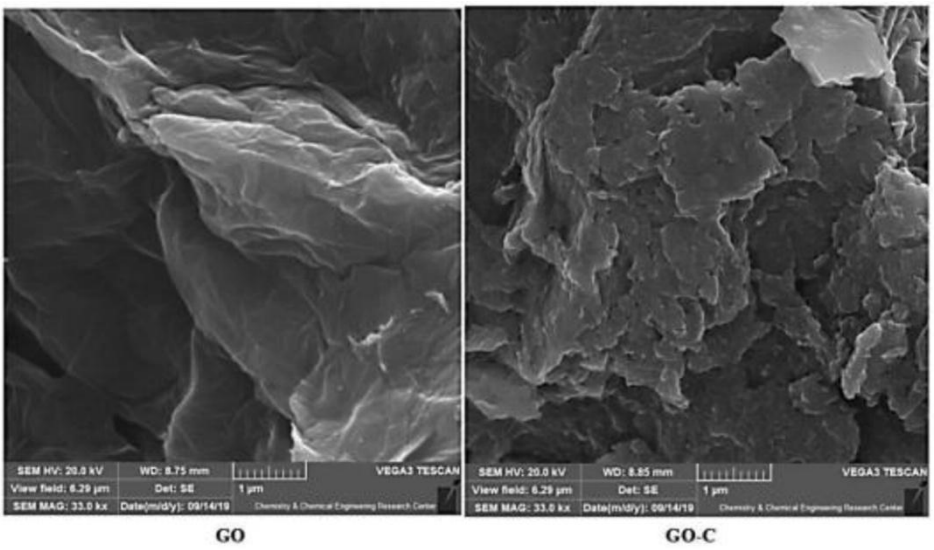

Fig. 1 — FESEM images of the GO and GO-C

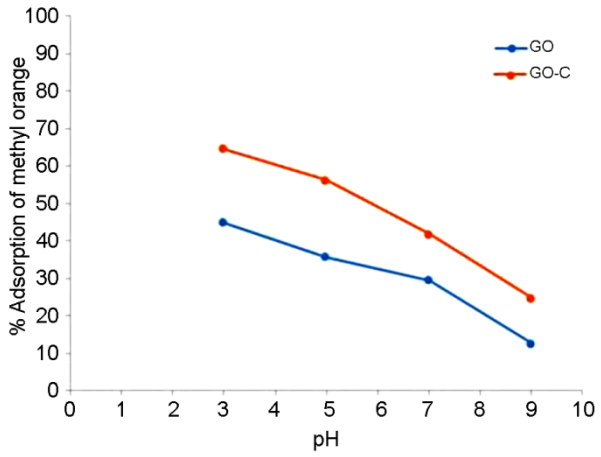

Fig. 2 — Effect of initial pH on methyl orange sorption onto GO and GO-C

taken up by the GO-C at pH 3 and 9 were 64.6% and 24.8%, respectively. At low pH values, the -NH_2 groups in the GO-C were converted to -NH_3^+ groups since the surface of the GO-C was positively charged. On the other hand, methyl orange has the quinoid structure (Fig. 3a) at this pH value. Hence, the quinoid structure of methyl orange is more easily adsorbed by GO-C than azo structure since the electrostatic attraction increases between the negatively charged methyl orange anions and the positively charged surface of GO-C that results in the removal of more methyl orange (Fig. 3b). In high pH values, the surface functional groups of GO-C dissociate to their anions which follow the negative or neutral charges on their surface. Therefore, the adsorption capacities decline due to the electrostatic repulsion between the negative charges of GO-C and methyl orange (azo structure) so that obtained adsorption percentage was very weak at pH=9 (Fig. 3a). Therefore, the adsorption of methyl orange got reduced at the high pH.

Sorption kinetic

Linear and nonlinear forms of kinetic models such as pseudo-first-order, which has been used for low concentration of solute proposed by Lagergren[32,47], pseudo-second-order[40], Elovich[48], (which describes chemisorption processes and usually utilized to the heterogeneous surfaces), were employed to investigate the rate of the adsorption process and rate-controlling step. These models were presented in Table 2. On the basis of the high R^2 and low RMSE values, the favorable kinetic model is selected. The parameters of k_1, q_e, q_t, k_2, a and b, which are shown in Table 2, are the adsorption rate constant of pseudo-first-order, the amount adsorbed at equilibrium, the amount adsorbed at time t, the pseudo-second-order rate constant of adsorption, the initial sorption rate, and the extent of surface coverage and activation energy for chemisorption, respectively.

As can be seen from Table 2, pseudo-second-order model of GO and GO-C shows high R^2 and low RMSE values for both forms of the linear and nonlinear in comparison with the pseudo first order model. Additionally, the adsorbed values of methyl orange at equilibrium (q_e) for GO and GO-C were found 76.92 and 111.11 mg g^{-1}, respectively, which approve well with the corresponded experimental data ($q_{e,ex}$= 74.78 and 107.67 mg g^{-1}). These results display

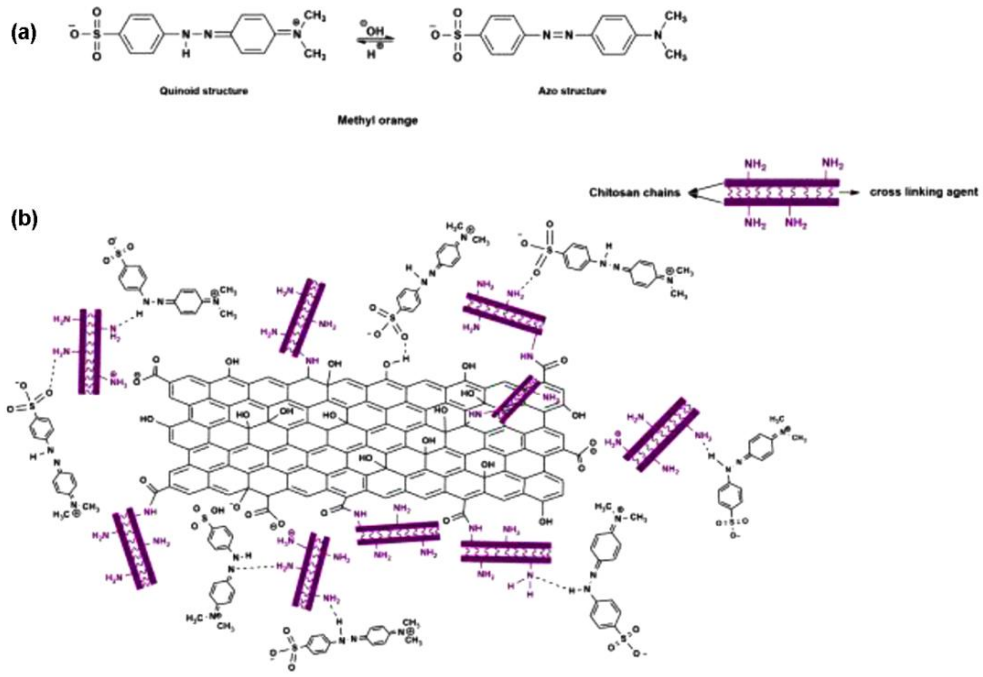

Fig. 3 — (a) The methyl orange structures in different pH and (b) Schematic for the mechanism for adsorption of methyl orange onto GO-C

Table 2 — Parameters of pseudo-first-order, pseudo-second-order, Elovich and intra-particle diffusion models for methyl orange sorption onto both adsorbents. Temperature, 298 K; initial methyl orange concentration, 100 mg L^{-1}; mass of adsorbents, 30 mg; volume of solution, 50 mL; and pH of the sample solution, 3.0

	Kinetic models	The calculated parameters				
	Pseudo-first-order	k_1 (min^{-1})	q_e(mg/g)	R^2	RMSE	Plot
GO	Linear $\log(q_e - q_t) = \log(q_e) - \frac{k_1}{2.303}t$	0.0702	24.89	0.7851	59.3	log (q_e - q_t) versus t
GO-C		0.0845	38.79	0.8249	82.1	
GO	Nonlinear $q_t = q_e(1 - e^{-k_1 t})$	2.507	66.12	0.1706	6.4	q_t versus t
GO-C		2.301	96.23	0.2402	8.9	
	Pseudo-second-order	K_2 (g mg^{-1} min^{-1})	q_e(mg/g)	R^2	RMSE	Plot
GO	Linear $\frac{t}{q_t} = \frac{1}{k_2 q_e^2} + \frac{1}{q_e}t$	0.0061	76.92	0.9968	10.6	t/$q_t$versus *t*
GO-C		0.0046	111.1	0.9978	13.6	
GO	Nonlinear $q_t = \frac{k_2 q_e^2 t}{1 + k_2 q_e t}$	0.0308	68.93	0.4319	5.3	q_t versus t
GO-C		0.0186	100.6	0.5284	7.0	
	Elovich	a	b	R^2	RMSE	Plot
GO	Linear $q_t = \frac{1}{b}\ln(ab) + \frac{1}{b}\ln(t)$	1.8×10^5	0.2006	0.7750	3.3	q_t versus ln t

(*Contd.*)

Table 2 — Parameters of pseudo-first-order, pseudo-second-order, Elovich and intra-particle diffusion models for methyl orange sorption onto both adsorbents. Temperature, 298 K; initial methyl orange concentration, 100 mg L^{-1}; mass of adsorbents, 30 mg; volume of solution, 50 mL; and pH of the sample solution, 3.0 (*Contd*.)

Kinetic models		Calculated parameters				
	Elovich	a	b	R^2	RMSE	Plot
GO-C		1.5×10^5	0.1322	0.8411	4.1	
GO	Nonlinear $q_t = \frac{1}{b}\ln(1+abt)$	2.4×10^4	0.1669	0.7431	3.3	q_t versus t
GO-C		2.3×10^4	0.1102	0.8074	4.1	
	Intra-particle diffusion	K_{id} (mg g^{-1} $min^{-0.5}$)		R^2	Plot	q_{ex}
GO	$q_t = k_{id}t^{0.5} + C_i$	2.862		0.8901	q_t versus $t^{1/2}$	74.78
GO-C		4.213		0.9095		107.67

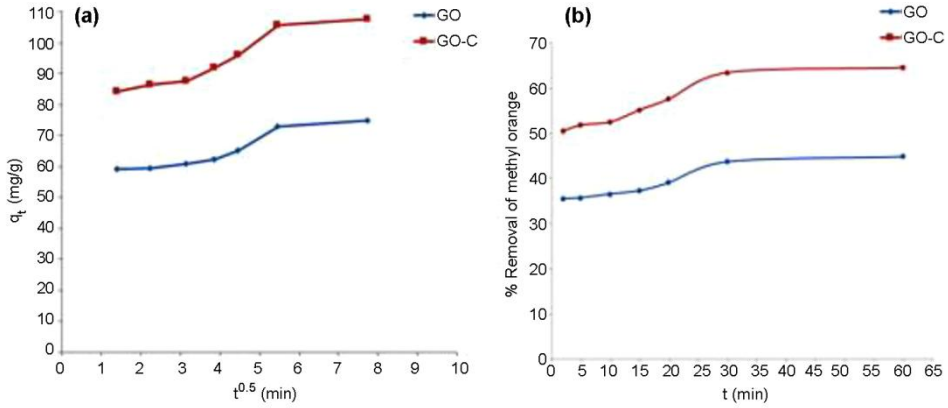

Fig. 4 — (a) Linearized intra-particle diffusion kinetic model of methyl orange sorption onto GO and GO-C and (b) Effect of contact time on the adsorption of methyl orange from aqueous solution by both adsorbents (experimental conditions: pH=3; adsorbent mass, 30 mg/50 mL; methyl orange concentration, 100 mg/L)

that the sorption of methyl orange from an aqueous solution onto both adsorbents obeys the pseudo-second-order kinetic model and could be utilized to determine the equilibrium sorption capacity, rate constants, and the removal percentage of methyl orange. On the other hand, although RMSE values of Elovich model for both adsorbents are low, their low determination coefficients for both forms signify inapplicablity of this model to fit the experimental data. Meanwhile, comparing the R^2 and RMSE values of two methods revealed that linear method provides better fitting of data and can present better description of parameters. Moreover, all plots of adsorption kinetics were presented in Supplementary Data, Figs S1-S3.

The other kinetic model is Weber-Morris intra-particle diffusion model which was used to the precise investigation and better understanding of the adsorption mechanism[33,49]. Actually, this model conveys the external mass transfer and intra-particle diffusion and expressed as follows in Eqn (5):

$$q_t = k_{id}\, t^{0.5} + C_i \quad \ldots (5)$$

where k_{id} (mole g^{-1} $min^{1/2}$) is the rate constant of intra-particle diffusion and C_i is proportional to the boundary layer thickness. If the regression of q_t versus $t^{1/2}$ gives a line that passes through the origin, then intraparticle diffusion is the sole rate-limiting step and k_{id} can be calculated from the slope and C_i from the intercept. Fig. 4a indicates the plot of the intra-particle kinetic model of methyl orange sorption by both the adsorbents. According to Fig. 4a, the plot has the nonzero intercept which shows intra-particle diffusion is not only the rate-controlling step of the sorption process. The difference in the rate of mass transfer during the initial and final stages of adsorption process can lead to the deviation of the straight line from the origin. Besides, the plots include

two different straight lines which show the mechanism of two stages for intra-particle diffusion of methyl orange within GO and GO-C. The initial adsorption stage starts from 0 to 30 min which is almost rapid. On the other hand, the second stage is milder and more gradual and is from 30 to 60 min for both adsorbents. These phenomena could be attributed to the fast diffusion of the methyl orange from the aqueous phase to the outer-surface of adsorbents for first stage and the intra-particle diffusion of the methyl orange molecules into the porous structure of adsorbent for the second stage. In other words, when the adsorption of exterior surface reached to saturation, methyl orange molecules enter into the pores of the adsorbent and were adsorbed by the interior surface. Totally, these results showed which both the external surface sorption and intra-particle diffusion contribute in the process of the methyl orange adsorption and that this model is not the only rate-controlling step. The calculated data are shown in Table 2.

Effect of contact time

The removal percentage of methyl orange by GO and GO-C was studied as a function of contact time, as shown in Fig. 4b. At up to 2 min of initial contact time, the adsorption percentage of methyl orange by GO and GO-C was found 35.5 % and 50.6%, respectively, which was rapid, and then reached equilibrium at nearly 30 min. In addition, their final values were calculated about 44.9% for GO and 64.6% for GO-C.The fast initial adsorption explains a high interaction of treated sorbent with methyl orange. The fast adsorption in the initial stage can be attributed to the presence of a huge number of vacant adsorption sites in which methyl orange molecules can easily interacted with these sites. After a period of time, the remaining available sites were difficult for the occupancy of methyl orange molecules which can be related to the repulsion between the adsorbed methyl orange molecules on the both adsorbents and bulk phases.

The dosage effect of adsorbent

The curves of the dosage effect of the adsorbents on the removal percentage of methyl orange from aqueous solution were illustrated in Fig. 5. The empirical findings showed a gradual increase in the removal of methyl orange with increasing the dosage of adsorbents from 0.01 to 0.07 g. This increase of the dosage considerably improved the removal percentage of methyl orange from 37.7% to 82.5% for GO and from 48.5% to 92.15% for GO-C. These results can be related to the fact that the dosage increment of adsorbents, in particular GO-C, makes more available adsorption sites for the methyl orange (Fig. 5).

Adsorption isotherms

Adsorption isotherms are the mathematical equations that show the relation between the adsorbate concentrations in the solid and liquid phases at a constant temperature. Furthermore, it explains when an equilibrium state is established in system, how a substance from the aqueous media transfers to a solid phase. In this study, the linear and nonlinear isotherm models of Langmuir, Freundlich, Halsey, Tempkin, Harkins-Jura and Dubinin-Radushkevich along with their calculated parameters, which describe the surface properties and affinity of the adsorbent, have been utilized to convey the mechanism of adsorption. All plots of adsorption isotherms are presented in Supplementary Data, Figs S4-S9.

Langmuir isotherm[41,50] assumes the completion of the monolayer coverage of the molecules on the adsorbent surface with no interaction between sorbed molecules with the same activation energy of adsorption and it is used for the homogeneous surface. Furthermore, multilayer adsorption and the heterogeneous surfaces with non-uniform distribution of adsorption heat are the features of Freundlich[51] and Halsey[52] isotherms. Additionally, Tempkin[53] model shows that the adsorption heat of all molecules linearly decreases with the surface coverage because of adsorbent-adsorbate interactions while Harkin-Jura[54] model conveys the existence of the

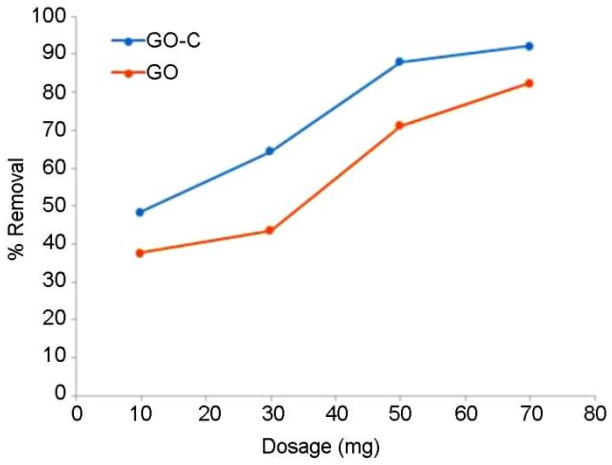

Fig. 5 — Effect of adsorbent dosage on the adsorption of methyl orange from aqueous solution (experimental conditions: pH 3, contact time 90 min, methyl orange concentration 100 mg/L, volume 50 mL)

heterogeneous pore distribution in the surface of adsorbents that it can be applied to the multi-layer adsorptions.

According to the Table 3, Langmuir isotherm is the best model for describing the adsorption of methyl orange by both adsorbents since this model indicates the highest R^2coefficient (> 0.99). In other words, the results explain that the Langmuir model well describes adsorption of methyl orange onto GO and GO-C. Moreover, the calculated parameters were somewhat different since linear and nonlinear methods were compared for Langmuir model. Although RMSE values of the nonlinear form were lower than linear form, the higher R^2 coefficients for

Table 3 — The parameters of the different isotherm models for methyl orange sorption from solution by GO and GO-C

Isotherm models		The calculated parameters				
Langmuir		q_m(mg/g)	b(L/mg)	R^2	RMSE	Plot
GO	Linear $\frac{C_e}{q_e}=\frac{1}{bq_m}+\frac{C_e}{q_m}$	77.52	0.4044	0.9988	2.5	$\frac{C_e}{q_e}$ vs.C_e
GO-C		111.11	0.8036	0.9901	23.35	
GO	Nonlinear $q_e=\frac{q_m bC_e}{1+bC_e}$	76	0.4833	0.9949	1.8	q_e vs. C_e
GO-C		97.48	6.673	0.8515	15.79	
Freundlich		K_f(mg/g)(mg/L)^n	n	R^2	RMSE	Plot
GO	Linear $\ln q_e=\ln K_f+\frac{1}{n}\ln c_e$	24.46	3.21	0.9034	9.7	ln q_e vs. ln C_e
GO-C		56.30	5.068	0.9606	8.7	
GO	Nonlinear $q_e=K_f C_e^{1/n}$	30.86	4.261	0.9181	7.3	q_e vs. C_e
GO-C		58.67	5.629	0.9594	8.3	
Halsey		K_H	$1/n_H$	R^2	RMSE	Plot
GO	Linear $\ln q_e=\frac{1}{n_H}\ln K_H-\frac{1}{n_H}\ln\frac{1}{C_e}$	3.5×10^{-5}	-0.3119	0.9034	63.9	lnq_e vs. ln $1/C_e$
GO-C		1.3×10^{-9}	-0.1973	0.9606	101.8	
GO	Nonlinear $q_e=\exp(\frac{\ln k_H-\ln C_e}{n})$	4.5×10^{-7}	-0.2347	0.9180	7.3	q_e vs. ln C_e
GO-C		7.3×10^{-9}	-0.2123	0.9459	8.5	
Tempkin		K_1(L/g)	K_2	R^2	RMSE	Plot
GO	Linear $q_e=K_1\ln K_2+K_1\ln C_e$	12.395	9.52	0.9798	3.6	q_e vs. ln C_e
GO-C		9.936	1029.96	0.9475	9.4	
GO	Nonlinear $q_e=K_1\ln(K_2C_e)$	12.39	9.52	0.9798	3.6	q_e vs. C_e
GO-C		9.936	1030	0.9475	9.4	
Harkins-Jura		A_{HJ}	B_{HJ}	R^2	RMSE	Plot
GO	Linear $\frac{1}{q_e^2}=\frac{B_{HJ}}{A_{HJ}}-\frac{1}{A_{HJ}}\log C_e$	625	1.562	0.7277	19.3	$1/q_e^2$ vs. log C_e
GO-C		1250	1.25	0.7797	30.2	
GO	Nonlinear $q_e=(\frac{A_{HJ}}{B_{HJ}-\log C_e})^{0.5}$	97.18	0.835	0.0806	26.7	q_e vs. log C_e
GO-C		87.63	0.5802	0.0978	42.9	
Dubinin-Radushkevich		q_m (mg/g)	K_{DR}	R^2 E(kJ/mol)	RMSE	Plot
GO	Linear $\ln(q_e)=\ln q_m-K_{DR}\varepsilon^2$	65.87	0.195	0.9378 1.6	9.7	ln q_e vs. ε^2
GO-C		88.10	0.0091	0.9019 7.4	19.7	
GO	Nonlinear $q_e=q_m e^{-K_{DR}\varepsilon^2}$	67.65	0.2602	0.8680 1.4	9.3	q_e vs. ε^2
GO-C		96.13	0.0253	0.8344 4.4	16.7	

linear method showed better fitting from it. Therefore, the linear method provides better fitting in estimating parameters. Meanwhile, the values of Langmuir parameters (b, q_m) are calculated and the related data are shown in Table 3. According to Table 2 and 3, the calculated q_e values had the considerable agreement with $q_{e.ex}$ values for both adsorbents which it confirmed Langmuir model for them. The essential features of the Langmuir model can be explained in terms of the separation factor or the equilibrium parameter R_L, which is defined as in Eqn (6):

$$R_L = \frac{1}{1+bC_0} \quad \text{... (6)}$$

where, b is the Langmuir constant and C_0 is the initial concentration of adsorbate in solution. The R_L values show the type of isotherm to be irreversible ($R_L = 0$), favorable ($0 < R_L < 1$), linear ($R_L = 1$) or unfavorable ($R_L > 1$). The calculated values of R_L for both adsorbents are shown in Table S1. The values of R_L in this work were found to be at around 0.01524–0.134041 for GO and 0.01229–0.11067 for GO-C, indicating a favorable behavior toward methyl orange adsorption. Other isotherm models did not have suitable fitting for interpretation of experimental data since R^2 values for both forms of linear and nonlinear were low.

On the other hand, Dubinin-Radushkevich (D-R) isotherm describes a Gaussian energy distribution onto a heterogeneous surface which it is utilized to explain the adsorption mechanism[37,55]. It can be calculated using the following linear relationship in Eqn (7):

$$\ln(q_e) = \ln q_m - k_{DR}\varepsilon^2, \quad \varepsilon = RT\ln\left(1+\frac{1}{C_e}\right) \quad \text{... (7)}$$

where q_e (mg/g) is the volume of methyl orange adsorbed, q_m (mg/g) is the maximum adsorption capacity of methyl orange, K_{DR} (mol^2/kJ^2) is the *D-R* isotherm constant, ε is Polanyi potential, R is the gas constant (0.008314 kJ/mol K), and T (K) is absolute temperature in Kelvin. In addition, the constant K_D presents the mean free energy, E (kJ/mol), of sorption per molecule of sorbate when it is transferred to the surface of the solid from infinity in the solution which can be calculated using the following expression in Eqn (8):

$$E = \frac{1}{\sqrt{2K_D}} \quad \text{... (8)}$$

In fact, the E value describes whether the adsorption on the GO and GO-C has happened as a physical or chemical process which it is important. On the basis of some papers[54,56], the adsorption process can be considered as the physical adsorption if the calculated value of E is below 8 kJ/mol but the chemical adsorption occurs in the range of 8-16 kJ/mol. Table 3 illustrates the estimated values of the D-R constants of the linear and nonlinear forms for both adsorbents. As can be seen from Table 3, the lower R^2 values and the proportion of relatively same RMSE in comparison to linear form for both adsorbents show the better agreement of linear form as compared to nonlinear form. Hence, the calculated values of E were found to be 1.6 kJ/mol for GO and 7.4 kJ/mol for GO-C. Then, it can be decided that physical adsorption may play a substantial role in the adsorption process of methyl orange on both adsorbents.

Thermodynamics analysis

The calculated thermodynamic parameters for adsorption of methyl orange by GO and GO-C are shown in Table 4. These parameters were estimated to investigate the spontaneity, feasibility and thermal properties of the adsorption process [57]. The ΔG^o value could be obtained from the following equation with the previous calculation of the adsorption equilibrium constant (K_C) as shown in Eqs. (9) and (10):

$$\Delta G^0 = -RT\ln(K_C) \quad \text{... (9)}$$

$$K_c = \frac{C_s}{C_e} \quad \text{... (10)}$$

Table 4 — The calculated thermodynamic parameters for the adsorption of methyl orange by both adsorbents

Adsorbents	T (K)	Kc	ΔG (KJ)	ΔH (KJ)	ΔS (KJ)
GO	298	0.8797	2.478	6.809	0.0219
	313	1.057	-0.144		
	323	1.079	-0.204		
GO-C	298	1.77	-1.414	7.173	0.0289
	313	2.086	-1.913		
	323	2.205	-2.124		

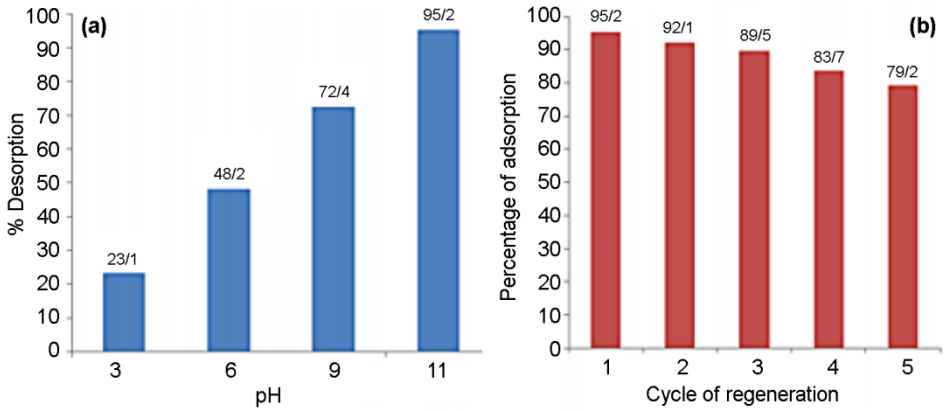

Fig. 6 — (a) The effect of solution pH on the methyl orange desorption from GO-C and (b) the regeneration of GO-C

where C_s (mg/L), R and T are the concentration of methyl orange on the adsorbent at equilibrium, the universal gas constant (8.314 J/mol K) and the temperature in Kelvin, respectively. In addition, the change in ΔSº and ΔHº at a constant temperature (T) can be found from the van't Hoff equation (Eqn (11)):

$$\ln K_c = (-\frac{\Delta H^0}{R})\frac{1}{T} + \frac{\Delta S^0}{R} \quad \text{... (11)}$$

The values of ΔSº and ΔHº were obtained from the intercept and slope, respectively of the linear plot of ln K_c versus *1/T*. The calculated values are given in Table 4. The results showed that the processes of adsorption of methyl orange onto both adsorbents are extremely favorable (negative values of ΔGº) under the conditions applied. Moreover, decreasing ΔGº values with increasing temperature confirms the feasibility and spontaneity of the methyl orange adsorption on the GO and GO-C. The positive values of ΔHº indicated the endothermic nature of the methyl orange adsorption on the both adsorbents. In fact, the increase of temperature causes more efficient adsorption of methyl orange on the adsorbents. The positive value of ΔSº demonstrated the increase in number of species at the solid-liquid interface and therefore an increasing randomness was observed at the solid-solution interface during the adsorption process of methyl orange onto the adsorbents.

Desorption performance of GO-C

The desorption experiments were carried out in different pH solutions since the desorption of methyl orange from GO-C is pH-dependent. Definitely, the adsorption and desorption are key parameters to evaluate an adsorbent because they can be reduced the total cost for application of the adsorbents. The desorption of methyl orange increased with increasing pH values. Besides, the desorption efficiency was calculated about 95.2% at pH = 11(Fig. 6a). The regenerated GO-C was reused for adsorption-desorption cycles and the data were shown in Fig. 6b. The results showed that the adsorption capacity of methyl orange on the GO-C was almost constant until the three regeneration cycle. Then, the adsorption capacity of methyl orange decreased for forth and five cycles (about 79%). Furthermore, it can be considered that the GO-C with significant stability can be used as an good reusable adsorbent for methyl orange.

Conclusions

We analyzed the adsorption process of methyl orange on the GO and GO-C. The results showed that GO-C has significant sorption capacity for methyl orange. The adsorption isotherms of methyl orange have been well fitted by Langmuir for both adsorbents. Meanwhile, ΔGº values were negative which show the practicability and spontaneity of the methyl orange adsorption. In addition, on the basis of ΔGº values and Dubinin-Radushkevich isotherm, the adsorption of methyl orange was physical. The sorption kinetics was found to follow pseudo-second-order model. Finally, the methyl orange desorption from the GO-C was about 95.2% which this result is meaningful since GO-C can be reused for further adsorption cycles.

Supplementary Data

Supplementary Data associated with this article are available in the electronic form at http://nopr.niscair.res.in/jinfo/ijca/IJCA_60A(02)209-219_SupplData.pdf.

Acknowledgement

The financial and encouragement support provided by Research Vice Presidency of Tehran Medical Sciences, Islamic Azad University.

References

1 Mittal A A, Kaur M D, Mittal J & Kurup L, *J Hazard Mater*, 148 (2007) 229.
2 Leon G, Garcia F, Miguel B & Bayo J, *Desalin Water Treat*, 57 (2016) 17104.
3 Munagapatia V S, Yarramuthib V & Kim D S, *J Mol Liq*, 240 (2017) 329.
4 Hosseini S, Khan M A, Malekbala M R, Cheah W & Choong T S Y, *Chem Eng J*, 171 (2011) 1124.
5 Choi H J & Yu S W, *Environ Eng Res*, 24 (2019) 99.
6 GerçelÖ, *Sep Sci Technol*, 51 (2016) 711.
7 Joseph J, Radhakrishnan R C, Johnson J K, Joy S P & Thomas J, *Mater Chem Phys*, 242 (2020) 122488.
8 Masoudian S, Rasoulifard M H & Pakravan P, *Indian J Chem*, 54A (2015) 757.
9 Zheng X, Zhang D, Gao Y, Wu Y, Liu Q & Zhu X, *Inorg Chem Commun*, 110 (2019) 107589.
10 Beluci N C L, Mateus G A P, Miyashiro C S, Homem N C & Vieira A M S, *Sci Total Environ*, 664 (2019) 222.
11 Herrero M & Stuckey D C, *Chemosphere*, 140 (2015) 119.
12 Isloor A M, Nayak M C I, Prabhu B & Asiri A M, *React Funct Polym*, 139 (2019) 170.
13 Zhou Y, Lu J, Zhou Y& Liu Y, *Environ Pollut*, 252 (2019) 352.
14 Wu Y, Su M, Chen J, Xu Z, Tang J, Chang X & Chen D, *Dyes Pigm*, 170 (2019) 107591.
15 Vidya J, John B A, Haribaaskar K&Balamurugan P, *Mater Sci Semicond Process*, 103 (2019) 104645.
16 Mohammad A T, Abdulhameed A S & Jawad A H, *Int J Biol Macromol*, 129 (2019) 98.
17 Darwish A A A, Rashad M & Hatem A A L Aoh, *Dyes Pigm*, 160 (2019) 563.
18 Uddin M K & Baig U, *J Clean Prod*, 211 (2019)1141.
19 Zhang B, Wu Y& Cha L, *J Dispers Sci Technol*, 41 (2020) 125.
20 Pérez-Ramírez E E, de la Luz-Asunción M, Martínez-Hernández AL, de la Rosa-Álvarez G, Fernández-Tavizón S, Salas P & Velasco-Santos C, *Carbon Lett*, 29 (2019) 155.
21 Robati D, Mirza B, Rajabi M, Moradi O, Tyagie I, Agarwal S & Gupta V K, *Chem Eng J*, 284 (2016) 687.
22 Subbaiah M V & Kim D S, *Ecotox Environ Safe*, 128 (2016) 109.
23 Rattanapan S, Srikram J & Kongsune P, *Energy Procedia*, 138 (2017) 949.
24 Rekha P, Muhammad R & Mohanty P, *RSC Adv*, 5 (2015) 67690.
25 Rekha P, Muhammad R, Sharma V & Ramteke M & Mohanty P, *J Mater Chem A*, 4 (2016) 17866.
26 Sharma V, Rekha P & Mohanty P, *J Mol Liq*, 222 (2016) 1091.
27 Muhammad R, Jyoti & Mohanty P, *J Mol Liq*, 248 (2017) 127.
28 Chaudhary M, Singh L, Rekha P, Srivastava V C & Mohanty P, *Chem Eng J*, 378 (2019) 122236.
29 Pal U, Sandoval A, Madrid S I U, Corro G, Sharma V & Mohanty P, *Chemosphere*, 163 (2016) 142.
30 Mekatel E H, Amokrane S, Aid A, Nibou D & Trari M, *C R Chim*, 18 (2015) 336.
31 Gan L, Shang S, Hu E, Yuen C W M & Jiang S X, *Appl Surf Sci*, 357 (2015) 866.
32 Li H, Sun Z, Zhang L, Tian Y, Cui G & Yan S, *Colloids Surf A Physicochem Eng Asp*, 489 (2016) 191.
33 Mahmoodian H, Moradi O, Shariatzadeh B, Salehf T, Tyagi I, Maity A, Asif M & Gupta V K, *J Mol Liq*, 202 (2015) 189.
34 Sui K, Li Y, Liu R, Zhang Y, Zhao X, Liang H & Xia Y, *Carbohydr Polym*, 90 (2012) 399.
35 Gao H, Song Z, Zhang W, Yang X, Wang X & Wang D, *J Environ Sci*, 53 (2017) 68.
36 Huang R, Hu C, Yang B & Zhao J, *Desalin Water Treat*, 57 (2016) 10646.
37 Munagapatia V, Yarramuthib V & Kima D, *J Mol Liq*, 240 (2017) 329.
38 Umpuch C & Sakaew S, *J Sci Technol*, 35 (2013) 451.
39 Wang Y, Xia G, Wu C, Sun J, Song R & Huang W, *Carbohydr Polym*, 115 (2015) 686.
40 Alimohammady M, Jahangiri M, Kiani F & Tahermansouri H, *Carbon Lett*, 29 (2019) 1.
41 MohseniKafshgari M & Tahermansouri H, *Colloids Surf B*, 160 (2017) 671.
42 Lai K C, Lee L Y, Hiew B Y Z, Thangalazhy-Gopakumar S & Gan S, *J Environ Sci*, 79 (2019) 174.
43 Yuan H, Meng L Y & Park S J, *Carbon Lett*, 17 (2016) 11.
44 Vakili M, Deng S, Cagnetta G, Wang W, Meng P, Liu D & Yu G, *Sep Purif Technol*, 224 (2019) 373.
45 Travlou N E, Kyzas G Z, Lazaridis N K & Deliyanni E A, *Chem Eng J*, 217 (2013) 256.
46 Baig N, Ihsanullah, Sajid M & Saleh T A, *J Environ Manage*, 244 (2019) 370.
47 Gholitabar S & Tahermansouri H, *Carbon Lett*, 22 (2017) 14.
48 Chien S H & Clayton W R, *Soil Sci Soc Am J*, 44 (1980) 265.
49 Weber W J & Morris J C, *J Sanit Eng Div*, 89 (1963) 31.
50 Langmuir I, *J Am Chem Soc*, 38 (1916) 2221.
51 Freundlich H M F, *J Phys Chem*, 57 (1906) 385.
52 Halsey G D, *Adv Catal*, 4 (1952) 259.
53 Tempkin M J & Pyzhev V, *Acta Physicochim URSS*, 12 (1940) 327.
54 Kausar A, Bhatti H N & Mackinnon G, *Colloids Surf B*, 111 (2013) 124.
55 Dubinin M M & Radushkevich LV, *Proc Acad Sci USSR Phys Chem Sect*, 55 (1947) 331.
56 Singha B & Das S K, *Colloids Surf B*, 107 (2013) 97.
57 Smith J M & Van Ness HC, *Introduction to Chemical Engineering Thermodynamics*, 6rd Edn., (McGraw-Hill, New York), 1987.